FOURIER BASED FAST MULTIPOLE METHOD FOR THE HELMHOLTZ EQUATION

C. Cecka* and E. Darve
Stanford University and Army High Performance Computing and Research Center
Stanford, CA 94305

ABSTRACT

The multilevel fast multipole method (MLFMM) is an algorithm that has had great success in reducing the computational time required to find the solution to the Galerkin boundary integral form of the Helmholtz equation. We present a new formulation of the MLFMM using Fourier basis functions rather than spherical harmonics in order to accelerate and simplify the time-critical stages of the algorithm. With modifications to the transfer function in the precomputation stage of the MLFMM, the interpolation and anterpolation algorithms become straightforward applications of FFT interpolations only. Using spectral methods, constructive algorithms are derived to determine a near-optimal quadrature for a given level in the algorithm and an a-priori estimate of the integration error.

1. INTRODUCTION

Since its development in (Rokhlin, 1990; Coifman *et al.*, 1993; Rokhlin, 1993; Engheta *et al.*, 1992; Rahola, 1996), the MLFMM has proven to be a very effective tool for solving acoustic and electromagnetic problems. We consider only the scalar wave equation, although any results can be extended to the vector case as described in (Chew *et al.*, 2001; Darve, 2000b). Applying the boundary integral method to the Helmholtz equation results in a dense linear system which can be solved by iterative methods such as GMRES or BCGSTAB. These methods require a dense matrix-vector product which, for a direct implementation, requires $\mathcal{O}(N^2)$ operations to compute. The MLFMM uses an approximation of the dense matrix to perform the product in $\mathcal{O}(N \log N)$ time. Computations taking advantage of this approximation are distributed through an oct-tree encompassing the domain of the scatterers to achieve the improved asymptotic running time.

There are a number of difficulties in implementing the MLFMM, each of which much be carefully considered and optimized to achieve the improved complexity. The largest complication is the quadrature sampling rate must increase with the size of the box in the oct-tree, requiring interpolation and anterpolation algorithms over the sphere to transform the data between quadratures. Local algorithms and interpolant matrix sparsifications are fast, but incur large errors. Fast transforms are available for spherical harmonics, but they are approximate, quite complicated to implement, and not always stable. We present the MLFMM and these choices in the next section.

2. THE MULTILEVEL FAST MULTIPOLE METHOD

The MLFMM improves the asymptotic complexity of the matrix-vector multiplication

$$\sigma_i = \sum_{j \neq i} \frac{e^{\imath\kappa|\mathbf{x}_i - \mathbf{x}_j|}}{|\mathbf{x}_i - \mathbf{x}_j|} \psi_j := \sum_j M_{ij} \psi_j \tag{1}$$

for $i, j = 1, \ldots, N$ from $\mathcal{O}(N^2)$ to $\mathcal{O}(N \log^2 N)$. This improvement is based on the Gegenbauer series

$$\frac{e^{\imath\kappa|\mathbf{r}+\mathbf{r}_0|}}{|\mathbf{r}+\mathbf{r}_0|} = \imath\kappa \sum_{n=0}^{\infty} (-1)^n (2n+1) G_n(\mathbf{r}, \mathbf{r}_0) \tag{2}$$
$$G_n(\mathbf{r}, \mathbf{r}_0) = h_n^{(1)}(\kappa |\mathbf{r}_0|) j_n(\kappa |\mathbf{r}|) P_n(\widehat{\mathbf{r}} \cdot \widehat{\mathbf{r}}_0)$$

where $h_n^{(1)}$ is the spherical Hankel function of the first kind, j_n is the spherical Bessel function of the first kind, and P_n is the Legendre polynomial of order n. The series converges absolutely and uniformly for $|\mathbf{r}| < |\mathbf{r}_0|$ and has been studied extensively in (Carayol & Collino, 2004; Darve, 2000a).

Truncating the Gegenbauer series at ℓ and using the identity

$$\int_{S^2} e^{\imath\kappa\mathbf{r}\cdot\mathbf{s}} P_n(\widehat{\mathbf{r}}_0 \cdot \mathbf{s}) \, dS(\mathbf{s}) = 4\pi\imath^n j_n(\kappa |\mathbf{r}|) P_n(\widehat{\mathbf{r}} \cdot \widehat{\mathbf{r}}_0)$$

where the integral is over the unit sphere $S^2 = \{\mathbf{s} \in \mathbb{R}^3 : |\mathbf{s}| = 1\}$, then

$$\frac{e^{\imath\kappa|\mathbf{r}+\mathbf{r}_0|}}{|\mathbf{r}+\mathbf{r}_0|} = \int_{S^2} e^{\imath\kappa\mathbf{r}\cdot\mathbf{s}} T_{\ell,\mathbf{r}_0}(\mathbf{s}) \, dS(\mathbf{s}) + \varepsilon_\ell \tag{3}$$

Report Documentation Page

Form Approved
OMB No. 0704-0188

1. REPORT DATE	2. REPORT TYPE	3. DATES COVERED
DEC 2008	**N/A**	**-**

4. TITLE AND SUBTITLE	5a. CONTRACT NUMBER
Fourier Based Fast Multipole Method For The Helmholtz Equation	5b. GRANT NUMBER
	5c. PROGRAM ELEMENT NUMBER
6. AUTHOR(S)	5d. PROJECT NUMBER
	5e. TASK NUMBER
	5f. WORK UNIT NUMBER
7. PERFORMING ORGANIZATION NAME(S) AND ADDRESS(ES) **Stanford University and Army High Performance Computing and Research Center Stanford, CA 94305**	8. PERFORMING ORGANIZATION REPORT NUMBER
9. SPONSORING/MONITORING AGENCY NAME(S) AND ADDRESS(ES)	10. SPONSOR/MONITOR'S ACRONYM(S)
	11. SPONSOR/MONITOR'S REPORT NUMBER(S)

12. DISTRIBUTION/AVAILABILITY STATEMENT
Approved for public release, distribution unlimited

13. SUPPLEMENTARY NOTES
See also ADM002187. Proceedings of the Army Science Conference (26th) Held in Orlando, Florida on 1-4 December 2008, The original document contains color images.

14. ABSTRACT

15. SUBJECT TERMS

16. SECURITY CLASSIFICATION OF:			17. LIMITATION OF ABSTRACT	18. NUMBER OF PAGES	19a. NAME OF RESPONSIBLE PERSON
a. REPORT	b. ABSTRACT	c. THIS PAGE			
unclassified	**unclassified**	**unclassified**	**UU**	**8**	

where we have defined the Gegenbauer truncation error ε_ℓ and the "transfer function"

$$T_{\ell,\mathbf{r}_0}(\mathbf{s}) = \frac{\imath\kappa}{4\pi}\sum_{n=0}^{\ell} \imath^n(2n+1)h_n^{(1)}(\kappa\,|\mathbf{r}_0|)P_n(\mathbf{s}\cdot\widehat{\mathbf{r}}_0). \quad (4)$$

Additionally, it will be useful to note the Jacobi-Anger series

$$e^{\imath\kappa\mathbf{r}\cdot\mathbf{s}} = \sum_{n=0}^{\infty} \imath^n(2n+1)j_n(\kappa\,|\mathbf{r}|)P_n(\mathbf{s}\cdot\widehat{\mathbf{r}}). \quad (5)$$

Consider two disjoint clusters of points $\{\mathbf{x}_i \mid i \in A\}$ and $\{\mathbf{x}_i \mid i \in B\}$ with radii $r_A \geq r_B \geq 0$ and centers $\mathbf{c}_A$ and $\mathbf{c}_B$ respectively. If $|\mathbf{c}_A - \mathbf{c}_B| > r_A$, then the matrix-vector product (1) is accelerated by using the approximation

$$\mathbf{M} \approx \begin{bmatrix} \mathbf{M}_{AA} & \mathbf{M}'_{AB} \\ \mathbf{M}'_{BA} & \mathbf{M}_{BB} \end{bmatrix}$$

where

$$\mathbf{M}_{AA} = [M_{ij}]_{i,j\in A}$$

$$\mathbf{M}'_{AB} = \left[\int_{S^2} e^{\imath\kappa\mathbf{s}\cdot\mathbf{r}_{ic}} T_{\ell,\mathbf{r}_0}(\mathbf{s}) e^{\imath\kappa\mathbf{s}\cdot\mathbf{r}_{cj}}\, dS(\mathbf{s})\right]_{i\in A, j\in B}$$

$$\mathbf{r}_{ic} = \mathbf{x}_i - \mathbf{c}_A, \quad \mathbf{r}_0 = \mathbf{c}_A - \mathbf{c}_B, \quad \mathbf{r}_{cj} = \mathbf{c}_B - \mathbf{x}_j$$

The improved asymptotic complexity of the FMM is achieved by constructing a tree of nodes $\{\mathbf{c}_p\}$, typically an octree, which partitions the support of the source and field points at the finest level. First, the outgoing plane-wave expansions due to the source points (or basis functions) are accumulated at the finest level in the tree. These outgoing expansions are then aggregated upward through the tree via additional plane-wave expansions. Incoming plane-wave expansions are computed from the outgoing by multiplication of the transfer function. These incoming plane-waves are then disaggregated downward through the tree. At the finest level the integration is performed and accumulated with the near field contribution to determine the field value at the field points (or testing functions).

2.1 Spherical Quadrature in the MLFMM

Noting the addition formula

$$(2n+1)P_n(\widehat{\mathbf{p}}\cdot\widehat{\mathbf{q}}) = 4\pi\sum_{m=-n}^{n} \overline{Y_n^m(\widehat{\mathbf{p}})}Y_n^m(\widehat{\mathbf{q}})$$

the transfer function (4) and Jacobi-Anger series can be expressed as

$$T_{\ell,\mathbf{r}_0}(\mathbf{s}) = \sum_{n=0}^{\ell}\sum_{m=-n}^{n} t_n^m Y_n^m(\mathbf{s}) \quad (6)$$

$$e^{\imath\kappa\mathbf{r}\cdot\mathbf{s}} = \sum_{n=0}^{\infty}\sum_{m=-n}^{n} e_n^m Y_n^m(\mathbf{s}) \quad (7)$$

Therefore, we wish to exactly integrate the spherical harmonics, Y_n^m. Below, we enumerate a number of choices for appropriate spherical quadratures that have previously been studied.

1. The simplest choice are sample points chosen uniformly in θ and ϕ. However, this choice does not accurately integrate the spherical harmonics and requires approximately twice as many points as the Gauss-Legendre quadrature below (Darve, 2000b).

2. The most common choice of sample points are uniform points for θ and Gauss-Legendre points for ϕ. With $N+1$ uniform points in the θ direction and $\frac{N+1}{2}$ Gauss-Legendre points in the ϕ direction, all Y_n^m, $-n \leq m \leq n$, $0 \leq n \leq N$ are integrated exactly (Darve, 2000b; Koc *et al.*, 1999).

3. McLaren in (McLaren, 1963) developed optimal choices of samples for general functions on S^2 based on equally spaced points and derived from invariants of finite groups of rotations. He also proposes a method for constructing equally weighted integration formulas on sets of any desired number of points by taking the union of icosahedral configurations.

2.2 Interpolation in the MLFMM

The quadrature sampling rate depends depends on the spectral content of the translation operator, $e^{\imath\kappa\mathbf{s}\cdot\mathbf{r}}$. This term's spherical harmonic coefficients e_n^m in (7) decreases super-exponentially roughly after the $\kappa\,|\mathbf{r}|$ mode, which scales linearly with the box size in the tree. Therefore, as we go up the tree in the aggregation step and $|\mathbf{r}|$ becomes larger, a larger quadrature and corresponding interpolation algorithm are required to resolve these higher modes. These modes must be resolved since they interact with the modes in the transfer function, which do not decay as ℓ increases.

Similarly, as we go down the tree in the disaggregation step, $|\mathbf{r}|$ becomes smaller, preventing the higher modes of the incoming field approximation from contributing to the integral as a consequence of Parseval's theorem. Thus, as the incoming field is disaggregated down the tree, a smaller quadrature can be used to resolve it. This makes the integration faster and is actually required to achieve an improved asymptotic running time at the cost of requiring anterpolation algorithms. Below, we enumerate a number of choices for interpolation and anterpolation algorithms that have previously been studied.

1. General interpolation algorithms for non-uniform grid points like Lagrange interpolation or B-

splines are fast and provide for simple error analysis. In (Koc *et al.*, 1999) it is shown that the error induced from Lagrange interpolation decreases exponentially as the number of interpolation points is increased for a given function of finite bandwidth. Thus, there is a trade-off between error and speed. The introduction of error is unavoidable with local schemes and is dependent on the values of the function at the time of interpolation.

2. For a set of quadrature points (θ_k, ϕ_k), $k = 1, \ldots, K$ with respective weights ω_k and corresponding function value f_k, a direct spherical harmonic transform sends f_k to a new quadrature $(\theta'_{k'}, \phi'_{k'})$, $k' = 1, \ldots, K'$ via the linear transformation

$$f_{k'} = \sum_{m,l \leq K} Y_l^m(\theta'_{k'}, \phi'_{k'}) \sum_k \omega_k \overline{Y_l^m(\theta_k, \phi_k)} f_k$$

This transform has nice properties analogous to those of the Fourier transform. A direct computation requires $\mathcal{O}(KK')$ operations which would result in an $\mathcal{O}(N^2)$ FMM. Fast spherical transforms (FST) have been developed in (Driscoll & Healy, 1994; Healy *et al.*, 2003; Rokhlin & Tygert, 2006) and applied to the FMM in (Chowdhury & Jandhyala, 2006). Using the FST reduces the interpolation and anterpolation procedures to $\mathcal{O}(K \log^2 K)$, which results in a $\mathcal{O}(N \log^2 N)$ MLFMM. However, the accuracy and stability of these algorithms are questionable as they rely on the nonequispaced discrete Fourier transform and/or the fast Legendre transform.

3. Approximations of the direct spherical transform have also been investigated in (Jakob-Chien & Alpert, 1997; Darve, 2000b). The interpolation matrix

$$A_{k'k} = \sum_{m,l \leq K} Y_l^m(\theta'_{k'}, \phi'_{k'}) \sum_k \omega_k \overline{Y_l^m(\theta_k, \phi_k)}$$

can be sparsified in a number of ways to provide an interpolation/anterpolation method that scales as $\mathcal{O}(K)$ with scalable relative error.

3. FOURIER BASED MLFMM

The Fourier based fast multipole method is based on the the identity

$$\int_{S^2} e^{\imath\kappa \mathbf{r}\cdot\mathbf{s}} T_{\ell,\mathbf{r}_0}(\mathbf{s})\, dS(\mathbf{s}) = \int_0^{2\pi}\int_0^{2\pi} e^{\imath\kappa \mathbf{r}\cdot\mathbf{s}} T^s_{\ell,\mathbf{r}_0}(\mathbf{s})\, d\theta d\phi \tag{8}$$

where $\mathbf{s} = [\cos(\theta)\sin(\phi), \sin(\theta)\sin(\phi), \cos(\phi)]$ and $T^s_{\ell,\mathbf{r}_0}$ is the "modified transfer function"

$$T^s_{\ell,\mathbf{r}_0}(\theta,\phi) = \frac{1}{2} T_{\ell,\mathbf{r}_0}(\mathbf{s})\, |\sin(\phi)| \tag{9}$$

Because the integrand is continuous and periodic, this formulation allows the use of the Fourier basis functions $\{e^{\imath n\theta} e^{\imath m\phi}\}$ which form an L^2 orthonormal set over $L^2([0, 2\pi] \times [0, 2\pi])$. Thus, we efficiently use two dimensional uniform quadratures, fast Fourier transforms in the interpolation and anterpolation steps, and spectral arguments in the error analysis. The result is a fast and easily implemented version of the MLFMM with strong control over the maximum absolute error, which we detail in the following sections.

3.1 Computing the Modified Transfer Function

Select a uniform quadrature with points (θ_i, ϕ_j) defined by

$$\theta_i = 2\pi \frac{i}{N_\theta} \qquad \phi_j = 2\pi \frac{j}{N_\phi}$$

Noting that the plane wave and modified transfer function both have spherical symmetry since

$$\mathbf{s}(\theta,\phi) = \mathbf{s}(\pi + \theta, 2\pi - \phi)$$

then the computational and memory cost will be reduced if the quadrature is also constructed with spherical symmetry since only half of the quadrature points will be need computed and stored. Thus, we force N_ϕ to be a multiple of 2 and N_θ to be a multiple of 4. By taking advantage of all of the symmetries of this quadrature the number of modified transfer functions that need to be precomputed is reduced from 316 per level to 34 - saving a factor of 9.3 in memory and costing a negligible permutation of values in time.

A key step to computing $T^s_{\ell,\mathbf{r}_0}$ is to remove the frequencies which a given quadrature cannot resolve. If $T^s_{\ell,\mathbf{r}_0}$ were simply sampled, significant frequency aliasing (or folding) would occur unless we used an unreasonably large quadrature. This is due to the slow decay of the Fourier series of $|\sin(\phi)|$,

$$\mathcal{F}(m; |\sin(\phi)|) = \frac{(-1)^m + 1}{\pi(1-m^2)} = \begin{cases} \frac{2}{\pi}\frac{1}{1-m^2} & \text{if } m \text{ even} \\ 0 & \text{if } m \text{ odd} \end{cases}$$

Since the spectrum of the plane-wave function

$$e^{\imath\kappa \mathbf{r}\cdot\mathbf{s}} = e^{\imath\kappa |\mathbf{r}| \cos(\theta_{\mathbf{s},\mathbf{r}})} = \sum_{n=-\infty}^{\infty} \imath^n J_n(\kappa\,|\mathbf{r}|) e^{\imath n(\theta_{\mathbf{s},\mathbf{r}})}$$

decays very rapidly for $n \gtrsim \kappa\,|\mathbf{r}|$, the high frequencies in $T^s_{\ell,\mathbf{r}_0}$ will not contribute to the final integral as a result of Parseval's theorem. By removing these frequencies from the modified transfer function, a smaller quadrature can be used without significantly affecting the total error.

Suppose we have chosen a quadrature characterized by (N_ϕ, N_θ). Since $T^s_{\ell,\mathbf{r}_0}$ is band-limited with bandwidth $2\ell+1$ in the θ-direction, we only need to treat the ϕ-direction carefully. Noting that $T_{\ell,\mathbf{r}_0}$ is bandlimited in ϕ with bandwidth $2\ell+1$, only frequencies $|m| \leq N_\phi/2 + \ell$ of $|\sin(\phi)|$ contribute to the $N_\phi/2$ frequencies of $T^s_{\ell,\mathbf{r}_0}$ resolved by the quadrature. Therefore, to compute a low-pass $T^s_{\ell,\mathbf{r}_0}$ we follow the algorithm sketched below:

For each θ_i, $0 \leq i < N_\theta/2$
$T_k \leftarrow \frac{1}{2} T_{\ell,\mathbf{r}_0}(\theta_i, \frac{2\pi k}{2\ell+1})$, $k = 0, \ldots, 2\ell$.
$\widetilde{T}_k \leftarrow$ Fourier series coefficient of T_k.
$\widetilde{s}_m \leftarrow \mathcal{F}(|m| \leq N_\phi/2 + \ell; |\sin(\phi)|)$.
$\widetilde{T}^s_n \leftarrow \widetilde{s}_m \otimes \widetilde{T}_k$ convolution of Fourier series.
$\widetilde{T}^s_n \leftarrow$ truncate to frequencies $|n| \leq N_\phi/2$.
$T^s(\theta_i, \phi_j) \leftarrow$ Inverse transform of $\widetilde{T}^s_n$.

This algorithm yields the low-pass modified transfer function at (θ_i, ϕ_j), $0 \leq i < N_\theta/2$, $0 \leq j < N_\phi$ which can be unwrapped to the remaining points by using the spherical symmetry

$$(\theta_i, \phi_j) = (\theta_{N_\theta/2+i}, \phi_{N_\phi - j}).$$

Note that this method can also be simply expressed in terms of Fourier interpolations and anterpolations. It is equivalent to making a Fourier interpolation of T_k to $(2\ell+1) + (2(N_\phi/2 + \ell) + 1) - 1$ points, multiplying by a low-pass $|\sin(\phi)|$ with frequencies $|m| \leq N_\phi/2 + \ell$, and performing a Fourier anterpolation back to N_ϕ points.

Finally, because sampling the transfer function at a single point is an $\mathcal{O}(\ell)$ operation, the algorithm as presented is $\mathcal{O}(\ell^3)$. The computation of the transfer function at all sample points can be accelerated to $\mathcal{O}(\ell^2)$ as in (Ergul & Gurel, 2006) by taking advantage of its symmetry about the $\widehat{\mathbf{r}}_0$ axis and using interpolation algorithms, but at the cost of introducing additional error.

3.2 Choice of Quadrature

The quadrature parameters can be constructively determined by deriving the maximum error they incur. The error in computing the integral with uniform quadrature is

$$|\varepsilon_I| = \left| \int_0^{2\pi} \int_0^{2\pi} e^{\imath\kappa\mathbf{r}\cdot\mathbf{s}} T^{\mathfrak{s}}_{\ell,\mathbf{r}_0}(\mathbf{s})\, d\theta d\phi - \sum_{m=1}^{N_\phi} \sum_{n=1}^{N_\theta} \omega_{n,m} e^{\imath\kappa\mathbf{s}_{n,m}\cdot\mathbf{r}} T^{\mathfrak{s},L}_{\ell,\mathbf{r}_0}(\mathbf{s}_{n,m}) \right|$$

where $\mathbf{s}_{n,m} = [\cos(\theta_n)\sin(\phi_m), \sin(\theta_n)\sin(\phi_m), \cos(\phi_m)]$ and $T^{\mathfrak{s},L}_{\ell,\mathbf{r}_0}(\mathbf{s}_{n,m})$ is the low-pass modified transfer function described in Sec. 3.1,

$$= \left| \int_0^{2\pi} \int_0^{2\pi} e^{\imath\kappa\mathbf{r}\cdot\mathbf{s}} \left(T^{\mathfrak{s},L}_{\ell,\mathbf{r}_0}(\mathbf{s}) + T^{\mathfrak{s},H}_{\ell,\mathbf{r}_0}(\mathbf{s}) \right) d\theta d\phi - \sum_{m=1}^{N_\phi} \sum_{n=1}^{N_\theta} \omega_{n,m} \left(E^L_{\kappa\mathbf{r}}(\mathbf{s}_{n,m}) + E^H_{\kappa\mathbf{r}}(\mathbf{s}_{n,m}) \right) T^{\mathfrak{s},L}_{\ell,\mathbf{r}_0}(\mathbf{s}_{n,m}) \right|$$

where $E^L_{\kappa\mathbf{r}}$ consists of the low frequencies of $e^{\imath\kappa\mathbf{r}\cdot\mathbf{s}}$ which are resolved by the quadrature and $E^H_{\kappa\mathbf{r}}$ consists of the high frequencies not resolved by the quadrature. Since $E^L_{\kappa\mathbf{r}} T^{\mathfrak{s},L}_{\ell,\mathbf{r}_0}$ is integrated exactly by a uniform quadrature,

$$= \left| \int_0^{2\pi} \int_0^{2\pi} E^H_{\kappa\mathbf{r}}(\mathbf{s}) T^{\mathfrak{s},H}_{\ell,\mathbf{r}_0}(\mathbf{s})\, d\theta d\phi - \sum_{m=1}^{N_\phi} \sum_{n=1}^{N_\theta} \omega_{n,m} E^H_{\kappa\mathbf{r}}(\mathbf{s}_{n,m}) T^{\mathfrak{s},L}_{\ell,\mathbf{r}_0}(\mathbf{s}_{n,m}) \right|$$

$$= \left| \int_0^{2\pi} \int_0^{2\pi} E^H_{\kappa\mathbf{r}}(\mathbf{s}) T^{\mathfrak{s},H}_{\ell,\mathbf{r}_0}(\mathbf{s}) - E^{\widehat{H}}_{\kappa\mathbf{r}}(\mathbf{s}) T^{\mathfrak{s},L}_{\ell,\mathbf{r}_0}(\mathbf{s})\, d\theta d\phi \right|$$

where we have denoted the aliased high frequencies of $e^{\imath\kappa\mathbf{r}\cdot\mathbf{s}}$ as $E^{\widehat{H}}_{\kappa\mathbf{r}}(\mathbf{s})$,

$$= \left| \int_0^{2\pi} \int_0^{2\pi} \left(E^H_{\kappa\mathbf{r}}(\mathbf{s}) - E^{\widehat{H}}_{\kappa\mathbf{r}}(\mathbf{s}) \right) T^{\mathfrak{s}}_{\ell,\mathbf{r}_0}(\mathbf{s})\, d\theta d\phi \right|$$

Transforming to Fourier space and applying the triangle inequality to prevent unpredictable cancelation effects,

$$\leq 4\pi^2 \sum_{n=-\ell}^{\ell} \sum_{m=-\infty}^{\infty} \left| \widetilde{E}(n,m) \right| \left| \widetilde{T}^{\mathfrak{s}}_{\ell,\mathbf{r}_0}(-n,-m) \right|$$

$$\widetilde{E}(n,m) = \widetilde{E}^H_{\kappa\mathbf{r}}(n,m) - \widetilde{E}^{\widehat{H}}_{\kappa\mathbf{r}}(n,m)$$

This remains an accurate upper bound due to the fast decay of $\widetilde{E}$ for sufficiently large values of N_θ and N_ϕ. See Fig. 1. Furthermore, this does not use phase information in computing the error, which accounts for more directional choices of $\mathbf{r}_0$ and $\mathbf{r}$ by taking advantage of the shift theorem.

3.2.1 Choosing N_ϕ

The worst case for ε_I in terms of N_ϕ occurs when $\mathbf{r}$ and $\mathbf{r}_0$ are aligned with the z-axis. This causes all spectral information to be contained in the ϕ-direction and makes ε_I a function of N_ϕ only. It leads to

$$|\varepsilon_I| \leq 4\pi^2 \sum_{m=-\infty}^{\infty} \left| \widetilde{E}^H_{\kappa\mathbf{r}}(0,m) - \widetilde{E}^{\widehat{H}}_{\kappa\mathbf{r}}(0,m) \right| \left| \widetilde{T}^{\mathfrak{s}}_{\ell,\mathbf{r}_0}(0,-m) \right|$$

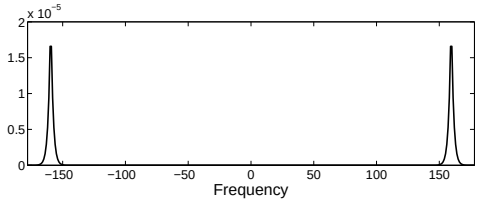

Fig. 1: The value of $\left|\widetilde{E}^{H}_{\kappa\mathbf{r}}(0,m) - \widetilde{E}^{\widehat{H}}_{\kappa\mathbf{r}}(0,m)\right|$ for $\kappa\,|\mathbf{r}| = 0.8\sqrt{3}\cdot 100$ and $N_\phi = 318$.

and applying the Jacobi-Anger identity,

$$e^{i\kappa\mathbf{s}\cdot\mathbf{r}} = \sum_{n=-\infty}^{\infty} i^n J_n(\kappa\,|\mathbf{r}|)e^{in\varphi}$$

where $\cos(\varphi) = \widehat{\mathbf{r}}\cdot\mathbf{s}$, this simplifies this to

$$|\varepsilon_I| = 4\pi^2 \sum_{m=-\infty}^{\infty} \left|J_{M(N_\phi,m)}(\kappa\,|\mathbf{r}|)\right| \left|\widetilde{T}^{\mathfrak{s}}_{\ell,\mathbf{r}_0}(0,m)\right| \quad (10)$$

where

$$M(N_\phi,m) = \begin{cases} N_\phi - |m| & |m| \le N_\phi/2 - 1 \\ |m| & |m| > N_\phi/2 - 1 \end{cases} \quad (11)$$

which can be used to efficiently search for a value N_ϕ via the following algorithm sketched below.

Choose N^n_ϕ sufficiently larger than $2\ell+1$.
$T_k \leftarrow T^s_{\ell,|\mathbf{r}_0|\widehat{\mathbf{z}}}(0, \frac{2\pi k}{N^n_\phi})$, $k = 0,\ldots,N^n_\phi - 1$.
$T_m \leftarrow$ absolute value of Fourier series of T_k.
$E_m \leftarrow |J_m(\kappa\,|\mathbf{r}|)|$.
For N_ϕ from 2ℓ to N^n_ϕ by 2
  $E^*_m \leftarrow E_{M(N_\phi,m)}$.
  If $E^*\cdot T < \varepsilon/4\pi^2$, return N_ϕ.

Since N^n_ϕ is typically only a small constant larger than $2\ell+1$, the algorithm as presented is dominated by the computation of the $\mathcal{O}(\ell)$ modified transfer function values and requires $\mathcal{O}(\ell^2)$ operations. Important optimizations include noting the symmetry $E^*_m = E^*_{-m}$ and $T_m = T_{-m}$ and also taking advantage of the very fast decay of J_n to accelerate the inner product by not including terms which cannot contribute. More advanced searching methods also provide improved performance.

3.2.2 Choosing N_θ

After determining an appropriate N_ϕ, a significant optimization is made by allowing N_θ to be a function of ϕ. This significantly reduces the number of quadrature points at negligible cost to the error. The worst case for the integration error occurs when $\mathbf{r}$ and $\mathbf{r}_0$ are in the xy-plane. Without loss of generality, suppose $\widehat{\mathbf{r}} = \widehat{\mathbf{x}}$. Then considering a constant $\phi = \phi_j$ and using the Jacobi-Anger identity, the plane wave can be expressed as

$$e^{\imath\kappa\mathbf{r}\cdot\mathbf{s}} = \sum_{n=-\infty}^{\infty} i^n J_n(\kappa\,|\mathbf{r}|\sin(\phi_j))e^{in\theta}$$

and noting that $J_n(\kappa\sin(\phi_j)\,|\mathbf{r}|)$ is exponentially small when

$$n \sim \mathcal{O}(\kappa\,|\mathbf{r}|\sin(\phi_j))$$

implying that we can truncate the series at $N_\theta(\phi_j) \sim \mathcal{O}(\kappa\,|\mathbf{r}|\sin(\phi_j))$ without incurring any appreciable error. Estimates of $N_\theta(\phi_j)$ can also be developed by determining when $J_n(\kappa\,|\mathbf{r}|\sin(\phi_j))$ is exponentially small, as in the computation of the excess bandwidth formula (EBF) in (Chew *et al.*, 2001). However, we find the EBF generated quadrature typically has an overestimated sampling rate.

First, it must be noted that letting N_θ be a function of ϕ_j requires an additional step in the computation of the modified transfer function. Sec. 3.1 computed the transfer function on a $N_\phi/2+1 \times N_\theta$ grid. With $N_\theta \to N_\theta(\phi_j)$, the data computed for each ϕ_j must be Fourier anterpolated from length N_θ to length $N_\theta(\phi_j)$.

To accurately and reliably compute $N_\theta(\phi_j)$ the same procedure as in Sec. 3.2.1 is applied but with $\mathbf{r}$ and $\mathbf{r}_0$ in the xy-plane. This represents the worst case for the integration error as a function of N_θ. For a given ϕ_j, we search for a $N_\theta(\phi_j)$ such that

$$|\varepsilon_I| \le 2\pi \sum_{n=-\ell}^{\ell} \left|J_{M(N_\theta(\phi_j),n)}(\kappa\,|\mathbf{r}|\sin(\phi_j))\right| \left|\widetilde{T}^{\mathfrak{s}}_{\ell,\mathbf{r}_0}(n;\phi_j)\right| \quad (12)$$

is bounded by a prescribed error. This is accomplished via the following sketched algorithm.

Set the poles $N_\theta(\phi_0) = N_\theta(\phi_{N_\phi/2}) = 1$.
Choose N^n_θ sufficiently larger than $2\ell+1$.
For ϕ_j, $j = 1,\ldots,N_\phi/2-1$
  $T_k \leftarrow T^s_{\ell,|\mathbf{r}_0|\widehat{\mathbf{x}}}(\frac{2\pi k}{2\ell+1},\phi_j)$, $k = 0,\ldots,2\ell$.
  $T_n \leftarrow$ absolute value of Fourier series of T_k.
  $E_n \leftarrow |J_n(\kappa\,|\mathbf{r}|\sin(\phi_j))|$.
  For $N_\theta(\phi_j)$ from 2 to N^n_θ by 2
    $E^*_n \leftarrow E_{M(N_\theta(\phi_j),n)}$.
    if $E^*\cdot T < \varepsilon/2\pi$, save $N_\theta(\phi_j)$ and $j \leftarrow j+1$.

Since N^n_θ is only a small constant larger than $2\ell+1$, the algorithm as presented is dominated by the computation of the modified transfer function and requires

$\mathcal{O}(\ell^3)$ operations. Again, using more advanced searching methods accelerates this algorithm and symmetry and decay properties of E^* and T should be use to improve the inner product computation. Using the EBF as an initial guess in the search for $N_\theta(\phi_j)$ further improves the searching speed. Additionally, only half of the $N_\theta(\phi_j)$'s should be computed due to symmetry.

3.2.3 Choosing $|\mathbf{r}|$ and $|\mathbf{r}_0|$

The previous algorithms require representative values of $|\mathbf{r}|$ and $|\mathbf{r}_0|$ for each level of the tree. The worst-case transfer vectors, $\mathbf{r}_0$, are well known to be those with minimum magnitude. If a_l is the box size at level l, then $|\mathbf{r}_0| = 2a_l$ is the smallest transfer vector length in the common one buffer box case.

The worst case values of $|\mathbf{r}|$ is well known to be the largest. For a box of size a_l, $|\mathbf{r}| \leq a_l\sqrt{3}$. However, using $|\mathbf{r}| = a_l\sqrt{3}$ in the previous methods is a very conservative choice. This case only occurs when two points are located in the exact corners of the boxes - rare indeed. See Fig. 2. Instead, we let $|\mathbf{r}| = \alpha a_l\sqrt{3}$ for some $\alpha \in [0, 1]$. A high α will strongly guarantee an upper bound on the error generated by the quadrature, but the points which actually generate this error become more and more rare. A lower value of α will yield a smaller quadrature, but more points may fall outside the radius $|\mathbf{r}|$ where the upper bound on the error is guaranteed. A typically reliable choice appears to be $\alpha = 0.8$. A study of this parameter will appear in a subsequent paper.

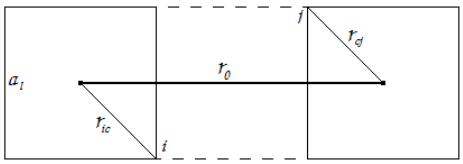

Fig. 2: The worst case $\mathbf{r}$ and $\mathbf{r}_0$, projected from the 3D box. Here, $|\mathbf{r}_0| = 2a_l$ and i and j on at opposite corners of the box so that $|\mathbf{r}| = |\mathbf{r}_{ic}| + |\mathbf{r}_{cj}| = a_l\sqrt{3}$.

3.2.4 Number of Quadrature Points

Recall from Sec. 2.1 that the typical approach in the standard MLFMM is to use $N+1$ uniform points in the θ direction and $\frac{N+1}{2}$ Gauss-Legendre points in the ϕ direction so that all Y_n^m, $-n \leq m \leq n$, $0 \leq n \leq N$ are integrated exactly. In (Koc *et al.*, 1999), Chew et. al. takes $\frac{N+1}{2} = \ell + 1$, which accounts for the rapid decay of the spherical harmonics in the plane wave expansion. This results in

$$M_g = 2(\ell + 1)^2 \approx 2\ell^2$$

quadrature points.

For a given Gegenbauer series truncation ℓ, the total number of active quadrature points required in the Fourier based MLFMM is approximately

$$M_f \approx \frac{N_\phi}{2}\frac{1}{\pi}\int_0^\pi N_\theta(\phi)\, d\phi \approx (\ell + C)\frac{2}{\pi}(2\ell + 1)$$

where $C \geq 1$ is a small integer dependent on ℓ numerically computed from the method in Sec. 3.2.1. Keeping only the dominant term,

$$M_f \approx \frac{4}{\pi}\ell^2$$

Thus, the method presented in this paper uses approximately 0.6 times the number of quadrature points in the standard MLFMM. However, it may be possible that the same N_θ optimization can be applied to the standard MLFMM for the same reasons it was applied in Sec. 3.2.2 to reduce the standard quadrature to a comparable size.

3.3 Interpolation and Anterpolation

Most importantly, the Fourier based MLFMM directly uses FFTs in the interpolation and anterpolation steps. This makes the time critical upward pass and downward pass especially fast and easy to implement.

Characterize a quadrature by an array of length $N_\phi/2 + 1$,

$$Q = [1, N_\theta(\phi_1), \ldots, N_\theta(\phi_{N_\phi/2-1}), 1]$$

noting that $N_\theta(\phi_j) = N_\theta(\phi_{N_\phi/2+j})$ and $N_\theta(\phi_j) = N_\theta(\phi_{N_\phi/2-j})$. A transform of the data $F(\theta_i, \phi_j)$ sampled on a quadrature Q to a quadrature Q' is performed by a sequence of Fourier interpolations and anterpolations. Let

$$\mathcal{N}_\theta = \max(\ \max_{0\leq j\leq N_\phi/2} N_\theta(\phi_j),\ \max_{0\leq j\leq N'_\phi/2} N'_\theta(\phi_j)\ )$$

Then, the following steps, as illustrated in Fig. 3, perform an exact interpolation/anterpolation using only FFTs.

1. For each ϕ_j, $0 \leq j \leq N_\phi/2$, Fourier interpolate the data $[F(\theta_{i=0,\ldots,N_\theta(\phi_j)-1}, \phi_j)]$ from length $N_\theta(\phi_j)$ to $\mathcal{N}_\theta$.
2. For each θ_i, $0 \leq i < \mathcal{N}_\theta/2$, wrap the data to construct the periodic sequence from the rest of the line $[F(\theta_i, \phi_{j=0,\ldots,N_\phi/2}), F(\theta_{i+\mathcal{N}_\theta/2}, \phi_{j=N_\phi/2-1,\ldots,1})]$.

3. For each θ_i, $0 \le i < \mathcal{N}_\theta/2$, Fourier interpolate the data $[F(\theta_i, \phi_{j=0,\ldots,N_\phi-1})]$ from length N_ϕ to N'_ϕ.

4. For each θ_i, $0 \le i < \mathcal{N}_\theta/2$, unwrap the data $[F(\theta_i, \phi_{j=0,\ldots,N'_\phi-1})]$ to construct the sequences $[F(\theta_i, \phi_{j=0,\ldots,N'_\phi/2})]$ and $[F(\theta_{i+\mathcal{N}_\theta/2}, \phi_{j=0,\ldots,N'_\phi/2})]$.

5. For each ϕ_j, $0 \le j \le N'_\phi/2$, Fourier anterpolate the data $[F(\theta_{i=0,\ldots,\mathcal{N}_\theta(\phi_j)-1}, \phi_j)]$ from length $\mathcal{N}_\theta$ to $N'_\theta(\phi_j)$.

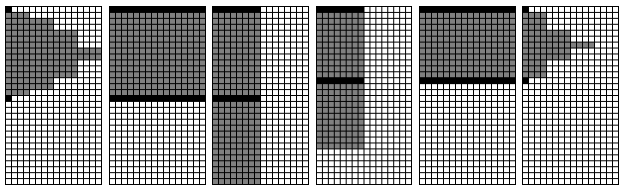

Fig. 3: The data profile at each step in an anterpolation from a large quadrature Q with $N_\phi = 30$ to a smaller quadrature Q' with $N'_\phi = 24$. The data corresponding to a pole has been darkened for clarity.

4. NUMERICAL RESULTS

A direct computation was used to compute the optimal Gegenbauer truncation ℓ and the methods described Sec. 3.2 were used to construct a quadrature. For a given box size s, the quadrature and truncation are constructed with $|\mathbf{r}| = 0.8s\sqrt{3}$, $|\mathbf{r}_0| = 2s$, and target error `eps`. The total measured error, ε, is

$$\varepsilon = \frac{e^{\imath\kappa|\mathbf{r}+\mathbf{r}_0|}}{|\mathbf{r}+\mathbf{r}_0|} - \sum_{m=1}^{N_\phi} \sum_{n=1}^{N_\theta(\phi_m)} \omega_{n,m} e^{\imath\kappa \mathbf{s}_{n,m}\cdot\mathbf{r}} T^{\mathfrak{s},L}_{\ell,\mathbf{r}_0}(\mathbf{s}_{n,m})$$

The total Gegenbauer truncation error, ε_G, is

$$\varepsilon_G = \frac{e^{\imath\kappa|\mathbf{r}+\mathbf{r}_0|}}{|\mathbf{r}+\mathbf{r}_0|} - \imath\kappa \sum_{n=0}^{\ell} (-1)^n (2n+1) G_n(\mathbf{r}, \mathbf{r}_0)$$

The total integration error, ε_I, is

$$\varepsilon_I = \varepsilon - \varepsilon_G$$

The plotted errors in Fig. 4 represent the maximum error found over many directions $\widehat{\mathbf{r}}$ and magnitudes $|\mathbf{r}| \le 0.8s\sqrt{3}$, where s is the box size.

Figure 5 shows the recorded running times of the Fourier based MLFMM and the direct matrix-vector product on a Intel Core(2) Quad CPU Q9450 2.66GHz with 4GB of RAM. Note that the intersection point is less than $N = 10,000$.

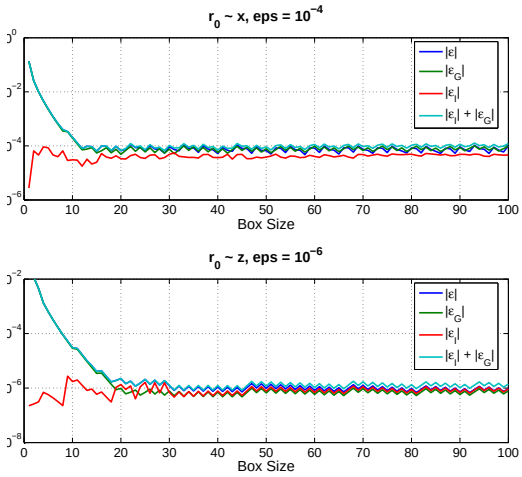

Fig. 4: Error of the FMM integral using a direct computation of ℓ and quadrature chosen as in Sec. 3.2.

5. CONCLUSIONS

We have proposed using a Fourier basis in the spherical variables θ and ϕ: $e^{\imath p\theta} e^{\imath q\phi}$. By modifying the Helmholtz kernel approximation and using a uniform quadrature we can take advantage of very fast, exact, and well-known FFT interpolation and anterpolation methods. By exploiting symmetries, the number of uniform quadrature points required is almost identical to the number of Gauss-Legendre quadrature points typically used for spherical quadratures and can be improved to use even fewer points. However, the Fourier based MLFMM requires careful changes to the precomputation stage where the modified transfer functions, $T^{\mathfrak{s}}_{\ell,\mathbf{r}_0}(\mathbf{s})$, are computed. Since $|\sin(\phi)|$ is not smooth, we must accurately precompute a band-limited version of the modified transfer function.

The Fourier based MLFMM approach has a number of advantages. Since the interpolation and anterpolation algorithms are exact, significant errors in the algorithm are a function of only the truncation parameter ℓ and the quadrature, specifically the bandwidth in the ϕ-direction. The truncation error ε_ℓ has been extensively studied and is well understood. The integration error ε_I can be accounted for during the precomputation stage and precise bounds on the final error can be made. The error analysis relies on well-known properties of the Fourier basis. We have used the results in constructive algorithms to determine the appropriate quadrature and constrain the MLFMM error a-priori. We find that bounding integration error is accurate and efficiently exploitable to search for the optimal quadrature. Although not required in the Fourier based MLFMM, computing the optimal quadrature can aid in error analysis and im-

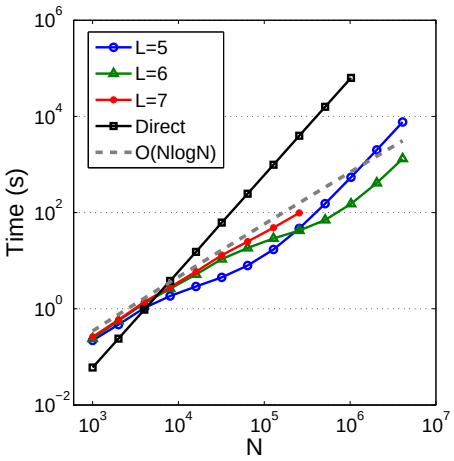

Fig. 5: Running times of the Fourier Based MLFMM with $\kappa \sim N^{1/3}$ such that for $N = 4 \times 10^6$ the points are uniformly distributed in a cube with side length 64λ.

prove performance. Since the Fourier Based MLFMM uses a uniform quadrature and well-known FFT algorithms, the time-critical stages of the algorithm are much easier to implement. Modern FFT packages are very common, extremely fast, numerically exact, and easy to use. FFTs scale much better than other fast interpolation algorithms of constant accuracy. Although the asymptotic complexity is not improved, the smaller constant in the FFT's $\mathcal{O}(N \log N)$ complexity yields improved running times in relation to algorithms of comparable accuracy.

References

Carayol, Q., & Collino, F. 2004. Error Estimates in the Fast Multipole Method for Scattering Problems. Part 2: Truncation of the Gegenbauer Series. *ESAIM: M2NA*, **39**(1), 183–221.

Chew, W.C., Michielssen, E., Song, J. M., & Jin, J. M. (eds). 2001. *Fast and Efficient Algorithms in Computational Electromagnetics*. Norwood, MA, USA: Artech House, Inc.

Chowdhury, Indranil, & Jandhyala, Vikram. 2006. Integration and Interpolation Based on Fast Spherical Transforms for the Multilevel Fast Multipole Method. *Microwave and Optical Technology Letters*, **48**(10), 1961–1964.

Coifman, R., Rokhlin, V., & Wandzura, S. 1993. The Fast Multipole Method for the Wave Equation: A Pedestrian Prescription. *Antennas and Propag. Magazine, IEEE*, **35**(3), 7–12.

Darve, Eric. 2000a. The Fast Multipole Method I: Error Analysis and Asymptotic Complexity. *SIAM J. Numer. Anal.*, **38**(1), 98–128.

Darve, Eric. 2000b. The Fast Multipole Method: Numerical Implementation. *J. Comput. Phys.*, **160**(1), 195–240.

Driscoll, James R., & Healy, D.M. 1994. Computing Fourier Transforms and Convolutions on the 2-Sphere. *Adv. Appl. Math.*, **15**(2), 202–250.

Engheta, N., Murphy, W. D., Rokhlin, V., & Vassiliou, M. S. 1992. The Fast Multipole Method (FMM) for Electromagnetic Scattering Problems. *IEEE Trans. Antennas Propag.*, **40**, 634.

Ergul, O., & Gurel, L. 2006. Optimal Interpolation of Translation Operator in Multilevel Fast Multipole Algorithm. *IEEE Trans. Antennas Propag.*, **54**(12), 3822–3826.

Healy, D.M., Rockmore, D., Kostelec, P.J., & Moore, S. 2003. FFTs for the 2-Sphere - Improvements and Variations. *J. Fourier Analysis and Applications*, **9**(4), 341–385.

Jakob-Chien, Rüdiger, & Alpert, Bradley K. 1997. A Fast Spherical Filter with Uniform Resolution. *J. Comput. Phys.*, **136**(2), 580–584.

Koc, S., Song, J. M., & Chew, W. C. 1999. Error Analysis for the Numerical Evaluation of the Diagonal Forms of the Scalar Spherical Addition Theorem. *SIAM J. Numer. Anal.*, **36**(3), 906–921.

McLaren, A. D. 1963. Optimal Numerical Integration on a Sphere. Oct.

Rahola, J. 1996. Diagonal Forms of the Translation Operators in the Fast Multipole Algorithm for Scattering Problems. *BIT*, **36**, 333–358.

Rokhlin, V. 1990. Rapid Solution of Integral Equations of Scattering Theory in Two Dimensions. *J. Comput. Phys.*, **86**(2), 414–439.

Rokhlin, V. 1993. Diagonal Forms of Translation Operators for the Helmholtz Equation in Three Dimensions. *Applied and Computational Harmonic Analysis*, **1**, 82–93.

Rokhlin, V., & Tygert, M. 2006. Fast Algorithms for Spherical Harmonic Expansions. *SIAM J. Scientific Computing*, **27**(6), 1903–1928.